Spin-Resolved Angle-Resolved Photoemission Spectroscopy: A Brief Overview

Austin de St Croix, Sydney Dufresne, Sebastian Gitt, Ryan Roemer

For PHYS 502, Dr. Mona Berciu, UBC

Submitted November 23rd 2018

1 Introduction

Angular-resolved photoemission spectroscopy (ARPES) is an experimental technique that allows for the determination of the electronic band structure of a material. This is typically done by illuminating the sample with ultraviolet light and measuring the angle of the emitted photoelectrons, which is proportional to their crystal momentum. The most common sources of high energy light for ARPES are synchrotron radiation and vacuum ultraviolet lasers, each of which have unique advantages and disadvantages. By polarizing the light from these sources, spin-dependent probing can be achieved in materials to investigate whether bands are spin-degenerate. In materials that lack inversion symmetry, the valence bands can split due to spin-orbit coupling, which can be detected with spin-resolved ARPES (SR-ARPES). This technique is an effective tool which can probe exotic materials such as topological insulators, which have nontrivial spin-polarized surface states.

2 Theory

2.1 ARPES

Photoemission spectroscopy (PES) experiments are based on the photoelectric effect, in which electrons are ejected from a sample using high energy radiation. This technique enables one to probe the electronic structure of materials by relating the energy and momentum of the photoemitted electron to the energy and momentum the electron had in the sample. Suppose an electron is excited by a photon with energy $h\nu$ into a state with momentum $\vec{k}$. The electron is ejected from the sample, and measured in vacuum as having energy ϵ_k and momentum $\vec{K}$ at an angle θ (Figure 1) relative to the surface normal. The kinetic energy of the photoemitted electron satisfies $\epsilon_k = h\nu - \phi - |E_B|$ where ϕ is the work function of the material, and E_B is the binding energy relative to the Fermi level E_F ($E_B = E(\vec{k}) - E_F$).

Conservation of momentum applies to the parallel components of momentum due to translational symmetry at the surface of the material [1] (see Appendix for discussion of perpendicular components).

$$k_{||} = K_{||} = \frac{\sqrt{2m\epsilon_k}}{\hbar}\sin(\theta) \tag{1}$$

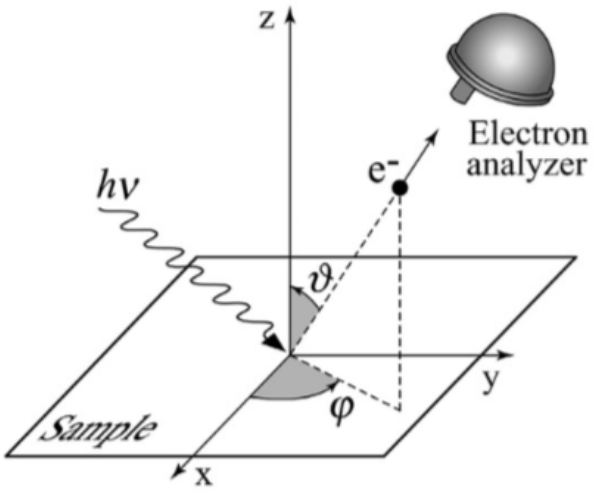

Figure 1: Schematic of APRES geometry. Emitted photoelectron direction is specified by (θ, ϕ) [2].

In experiments, the photoemitted electron intensity (or photocurrent) for a given range of energies and angular distributions is the quantity being measured by ARPES. Starting with a N-electron system, incident radiation will excite an electron in a single-particle state ϕ_i to a state ϕ_f, where we separate the remaining (N-1)-electron states before ($\Psi_i^{(N-1)}$) and after ($\Psi_f^{(N-1)}$) removal of the electron. The total transition probability per unit time, associated with the time-dependent perturbation $\hat{H}_{int} \propto \vec{A}\cdot\vec{p}$, is given by Fermi's Golden Rule (see Appendix for derivation)

$$I = \Sigma_{i,f} w_{i\to f} \tag{2}$$

where

$$w_{i\to f} \propto \Sigma_s |\langle \Psi_{f,s}^{(N-1)} | \Psi_i^{(N-1)} \rangle|^2 |M_{i,f}|^2 \delta(E_f - E_i - h\nu) \tag{3}$$

where $|M_{i,f}| = |\langle \phi_f(\epsilon_k, \vec{k}) | (\vec{\epsilon}\cdot\vec{r}) | \phi_i(\vec{k}_i) \rangle|$ is the ARPES matrix element [1]. The final (N-1)-electron state may contain a range of electron and quasiparticle excitations ($\Psi_{f,s}^{(N-1)}$) depending on the strength of electron-electron, electron-phonon, etc., interactions in the system. All of these interactions are described by a continuous function known as the spectral function $A(\vec{k},\omega)$ (related to the $|\langle \Psi_{f,s}^{(N-1)} | \Psi_i^{(N-1)} \rangle|$ term in Eq. 3)

$$A(\vec{k},\omega) = \frac{1}{\pi}\frac{\mathrm{Im}(\Sigma(\vec{k},\omega))}{(\hbar\omega - \epsilon_k^0 - \mathrm{Re}(\Sigma(\vec{k},\omega)))^2 + \mathrm{Im}(\Sigma(\vec{k},\omega))^2} \tag{4}$$

$\Sigma(\vec{k},\omega)$ is known as the self-energy. The self-energy is a complex function that has real and imaginary parts corresponding to a shift in the electron energy in the band ϵ_k^0 due to interactions, and the lifetime of the quasi-particle, respectively [3]. In the case of non-interacting systems, the self-energy is zero and the spectral function reduces to a delta function centered at the band energy ϵ_k^0. In the interacting case close to the Fermi surface (where $\epsilon_k^0 - \mu >> |\mathrm{Im}(\Sigma(\vec{k},\omega))|$, as in the case of a Fermi liquid), one can then expand the spectral intensity (Eq. 13) about the poles. The singular and non-singular terms of this expansion correspond to the coherent (main line, quasiparticle peak) and incoherent (satellite parts of the spectral intensity), respectively.

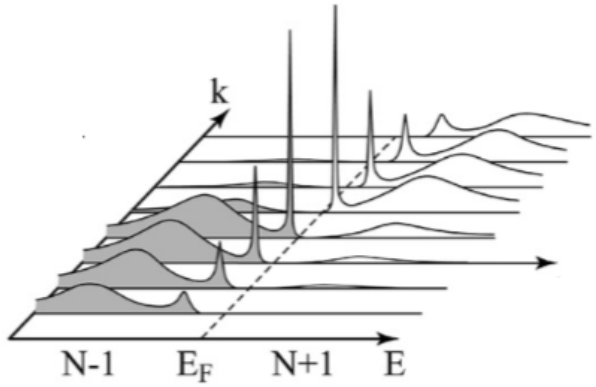

Figure 2: Spectral distribution peaks as a function of wavevector $\vec{k}$ and energy E near the Fermi energy. The in coherent part of the spectrum broadens, while the quasiparticle lifetime grows as the Fermi energy is approached [2].

Spectral intensity ($I(\vec{k},\omega) \propto \Sigma_{i,f,s}|M_{i,f}|^2 A(\vec{k},\omega)$) measured as a function of momentum $\vec{k}$ is known as an energy distribution curve (EDC). Peaks in these curves correspond to high photoelectron densities indicating the center of an electron band, while the widths of these peaks correspond to the lifetimes of quasiparticles, as shown in Figure 2.

2.2 Spin Polarization

SR-ARPES experiments take advantage of the spin-dependence in scattering experiments to characterize the spin-polarization $P(\vec{k},\omega)$ of electrons with momentum $\vec{k}$ measured with the spectrometer:

$$P(\vec{k},\omega) = \frac{I_\uparrow(\vec{k},\omega) - I_\downarrow(\vec{k},\omega)}{I_\uparrow(\vec{k},\omega) + I_\downarrow(\vec{k},\omega)} \tag{5}$$

where $I_{\uparrow\downarrow}(\vec{k},\omega)$ is the SR-ARPES spectrum corresponding to a particular spin axis [4].

3 Light Source

Synchrotron radiation is a common source of light for SR-ARPES experiments. Beams can be produced by the cyclotron-motion of electrons about a constant magnetic field along a circular track. Another common technique is the use of undulators, which are periodically spaced magnets with fields in opposing directions, causing the electrons to oscillate as they travel down a path [5]. Diagrams of the two different types can be seen in Figure 3. In both cases, this acceleration causes the electron to emit photons, which are sent down beam lines to be used for experiments. Synchrotrons produce photons with an energy range of approximately 20-200 eV, but a grating monochromator can be used to select narrower bands of frequencies [6]. Any arbitrary polarization can be achieved from synchrotrons using wave-plates [7].

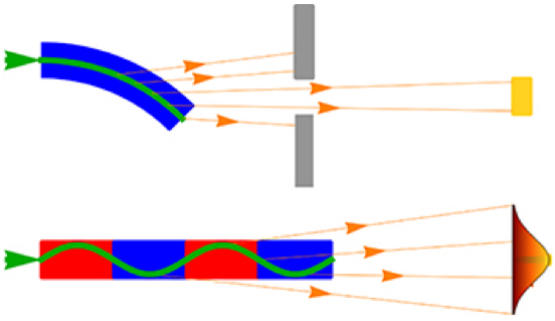

Figure 3: Diagrams of the bending magnet (top) and wiggler (bottom) synchrotron designs, as well as their corresponding output [8].

Another common source of light for SR-ARPES are solid-state vacuum ultraviolet lasers, which are capable of providing photon energies of around 5-7 eV, exceeding the work function of most materials [9]. Typically, frequency quadrupling of Ti:sapphire lasers (through non-linear effects in crystals such as β-barium borate) are used to produce photon energies of 6 eV [10]. Unlike synchrotron sources, these

lasers are not tunable, but they do have a much higher energy (momentum) resolution due to their lower photon energy. Laser-based ARPES systems have been demonstrated with photon energy resolution as low as 0.26 meV, while state-of-the-art synchrotron sources only reach as low as 4 meV [11][9]. Another advantage of using lower energy photons is that it restricts emitted electrons to the first Brillouin zone, reducing background noise due to scattering.

Furthermore, lasers are able to provide photon fluxes on the order of 10^{15} photons/s, which is at least two orders of magnitude higher than fluxes provided by modern synchrotron sources. This greatly improves the signal-to-noise ratio [11]. Both laser and synchrotron sources are capable of achieving spot sizes down to 0.2 mm [9].

If too many photoelectrons are ejected simultaneously, they will experience a Coulombic repulsion known as the space charge effect, introducing an uncertainty into the final momentum measurement [13]. For this reason, Ti:sapphire lasers use pulses of a few picoseconds, as opposed to tens of femtoseconds, which is a limitation in studying time-resolved electron dynamics. Systems using synchrotrons experience much greater space charge effects, which can be attributed mostly to their larger energy bandwidth [9].

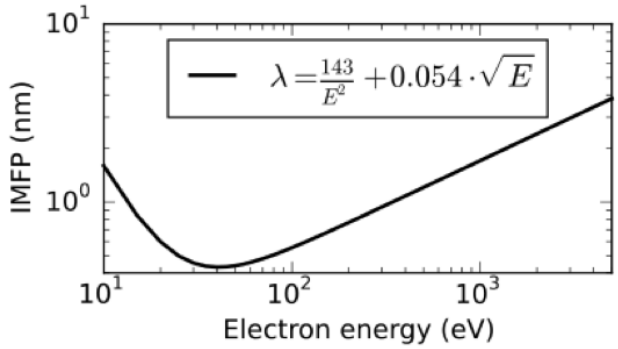

Figure 4: Inelastic mean free path vs. electron energy relation that is approximately valid for most materials [12].

Another important consideration is the inelastic mean free path (IMFP) of the emitted electron, which describes how far an electron will travel through a solid before losing its kinetic energy due to collisions, resulting in the formation of electron-hole pairs, phonons, and plasmons [14]. The mean free path is approximately the same for different materials, instead varying primarily due to the kinetic energy of the electron [12]. As seen in Figure 4, the mean free path is the smallest for energies in the 20-100 eV range, which is the main operating range of synchrotron sources.

Ultraviolet lasers are therefore capable of penetrating further into the material, with depths up to 3-10 nm, while synchrotrons are only go to depths of 0.5-2 nm, limiting them to surface states [9].

4 Detector

Compared to traditional ARPES, spin resolved measurements must sacrifice some energy and momentum resolution to resolve the photoelectron's spin in addition to $\vec{K}$ and E. This is due to the more complex electron detector which typically involves the electrons undergoing an additional scattering event before detection.

The following discussion pertains to both traditional and spin resolved ARPES. In this low energy photon-electron scattering there is no biasing between the lab frame and center of momentum frame [15]. Because of this, the detector is usually rotated relative to the sample at a fixed radius. A sketch of the experimental setup is shown in Figure 5, where the electron detector measures the scattering angle θ in the mirror plane. It is important that the sample be properly aligned with respect to the incoming photons such that ϕ and θ properly reflect the scattering angles. If not, the components of $K_{||}$ will be rotated and erroneous in magnitude ($|K_{||}| \propto \sin\theta$).

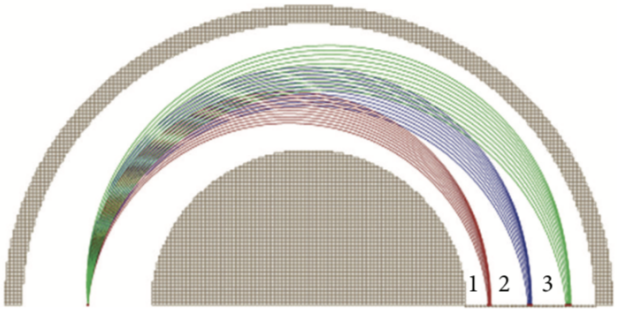

Figure 5: A SIMION simulation showing how electrons with different energy behave in the half-sphere electron detector. The outer shell is at negative potential while the inner shell is positively charged. Taken from [16].

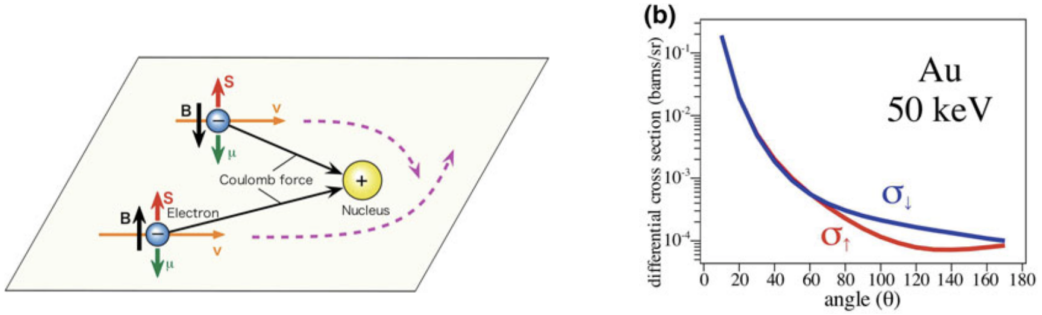

Figure 6: Left: The incoming electrons scatter to either side depending on their spin coupling with the induced $\vec{B}$ field. Right: The Mott effect is dominant at $\theta \approx 120^o$ in the differential cross section, this example for 50 keV electrons impinging on gold. Image adapted from [18].

Upon entering the detector the electrons are first collimated using a series of electrostatic lenses (analogous to focusing light)[1]. A half sphere electron deflector is then used to select the energy of the photoelectrons. The outer and inner spheres (with radius R_{out} and R_{in}) are held at potential difference ΔV. Highly energetic electrons will not be sufficiently deflected while low energy electrons are attracted to the inner sphere (at positive potential). The energy of surviving electrons E, and energy resolution ΔE are given by the formulas below, where the slit width $a = R_{out} - R_{in}$ and $\Delta\theta$ is the polar acceptance angle of the detector (with respect to the sample) [17].

$$\begin{aligned} E &= \frac{e\Delta V}{\frac{R_{in}}{R_{out}} - \frac{R_{out}}{R_{in}}} \\ \Delta E &= E\left[\frac{2a}{R_{in}+R_{out}} + (\frac{\Delta\theta}{2})^2\right] \end{aligned}$$

Before entering the deflector, a retarding potential can be applied to lower E and improve the energy resolution. The expression above for ΔE is for a perfectly monochromatic light source, but in reality the bandwidth of the laser must be convolved with the detector's resolution to give a total energy resolution. The momentum resolution is approximately given by $\Delta k_{||} \approx \sqrt{2mE/\hbar^2}\cos\theta\Delta\theta$. In ARPES a continuous dynode or multi-channel electron multiplier (electron counter) will be placed at the exiting end of the deflector to count the electrons.

In spin resolved measurements an additional complexity is required before counting electrons. The most common technique[2] uses Mott scattering, a spin-orbit interaction, to resolve spins. After passing through the deflector described above the electrons are accelerated to $\sim$ 100keV before impinging upon a thin film of high Z material (typically a noble metal, such as gold). The electrons penetrate to the metal's nucleus and see a net positive charge which induces a magnetic field [18].

$$\vec{B} = -\frac{1}{c}\vec{v}\times\vec{E} = \frac{Ze}{cr^3}\vec{r}\times\vec{v} = \frac{Ze}{mcr^3}\vec{L} \qquad (6)$$

Where $\vec{E} = \frac{Ze}{r^3}\vec{r}$ was used. The electron's spin will couple with this magnetic field through the dipole interaction:

$$V_{LS} = -\vec{\mu}\cdot\vec{B} = \frac{Ze^2}{2m^2c^2r^3}\vec{L}\cdot\vec{S} \qquad (7)$$

This spin-orbit potential will pull the electron to one side or another depending on the spin, as seen in Figure 6. However this effect is weak and cannot be easily resolved at all scattering angles or energies. The effect becomes more prominent at higher energies and when the electrons back-scatter off the foil at about $\theta \approx 120^o$. At low energy the electron cloud shields the nucleus reducing the Mott effect, and for softer scattering angles the electron is likely to multi-scatter. As θ approaches 180^o $\vec{L}$ decreases, also weakening the spin-orbit potential V_{LS}. At very high energies brehmsstrahlung and other effects occur, so these detectors must operate within these limits to minimize other non-Mott scattering effects.

[1] It is interesting to note that the particle density of the electron beam in the phase space $(\vec{r},\vec{p})$ is conserved by Liouville's theorem. Performing collimation will increase the momentum spread but the product of momenta and displacement for the beam population will remain constant

[2] Very Low Energy Electron Diffraction, VLEED, is becoming more popular in the field. It utilizes spin exchange interactions with spin-polarized copper-oxides to resolve spin. It works with much lower voltage and has a better signal to noise ratio compared to Mott detectors.

Two electron counters are placed at $\pm 120^o$ from the gold foil, each one measuring a given spin polarization. This second scattering event reduces the total number of electrons measured by a factor of $10^{-3} - 10^{-4}$ leading to a reduced intensity. A retarding potential can be added to deflect multi-scattered (lower energy) electrons which allows the detectors to be made smaller as lower potentials are needed. SR-ARPES detectors operate with energy resolutions on the order of 10 meV and angular resolution of about one degree, although it varies greatly from one system to another. This detector provides a precise method to measure the complete state of electrons near the surface of materials.

5 A Motivating Example

Topological states are interesting because the preserved time reversal symmetry (the Hamiltonian commutes with the time reversal operator) at the surface guarantees conductance due to the elimination of back-scattering. Topological states are realized when Kramer's degeneracy is broken, implying a splitting in the energies of spin states predicted by Kramer's theorem. This theorem states that spin $\frac{1}{2}$ particles will have degenerate energy eigenstates. This energy splitting may be complemented by momentum dependent splitting known as the Rashba effect, where spin-orbit coupling and asymmetry in the crystal structure (specifically in the direction perpendicular to the proving surface) are responsible.

SR-ARPES allows for the direct probing of the spin polarization of energy bands with high momentum resolution. Because of the net zero spin polarization of the system it is difficult to show any spin dependence. This technique proves extremely useful when considering the spin states in such materials where the surface or edge bands are distinct from that of the bulk. In these systems it is not only the linear dispersion of the bands that is unique but the projection of the spin. Fundamentally, this is due to the spin orbit interaction inverting the bulk bands, which causes an energy gap.

In addition to spin-orbit coupling topological states are often realized in materials with small band gaps. Significant change to the electronic structure is brought about via the spin-orbit interaction typically introduced as a small perturbation. Thus one should look low on the periodic table for constituent candidates for topological materials, where the relativistic effect of spin-orbit coupling is greatest. Here we discuss an archetypal compound, Bi_2Se_3 to develop an idea of the insight gained from SR-ARPES.

5.1 Bismuth Selenide Bi_2Se_3

Hexagonal Bi_2Se_3 with a band gap of $\sim$220 meV has been suggested to host topologically non-trivial states centered around the gamma point (center of the Brillouin Zone). In this region the boundary between the topological trivial vacuum states (Chern number is equal to zero) and the non-trivial bulk states (Chern number is non-zero) gives rise to non-trivial surface states where Kramers degeneracy is lifted. A toy description of these bands can be seen in Figure 7 where a cut through the gamma point reveals that the bulk valence band and bulk conduction bands are gapped, but the topological surface states are continuous. These spin-split states will again be degenerate at the Dirac point where the spin up and spin down bands overlap.

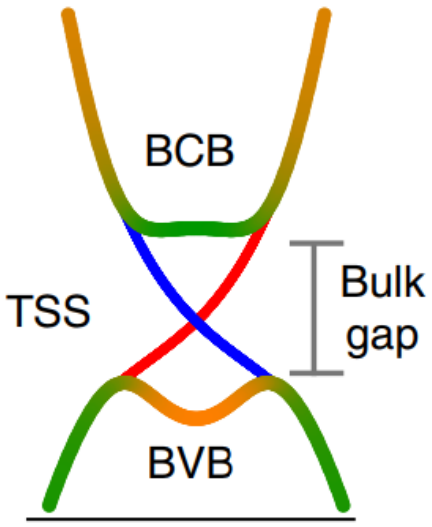

Figure 7: A toy model of the electronic structure of Bi_3Se_3. The bulk conduction band (BCB) and bulk valence band are gaped where the topological surface state (TSS) is present within the bulk energy gap. Note the m-shape of the BVB which is a tell tale sign of band inversion [19]. At this point ignore the colour of the bands.

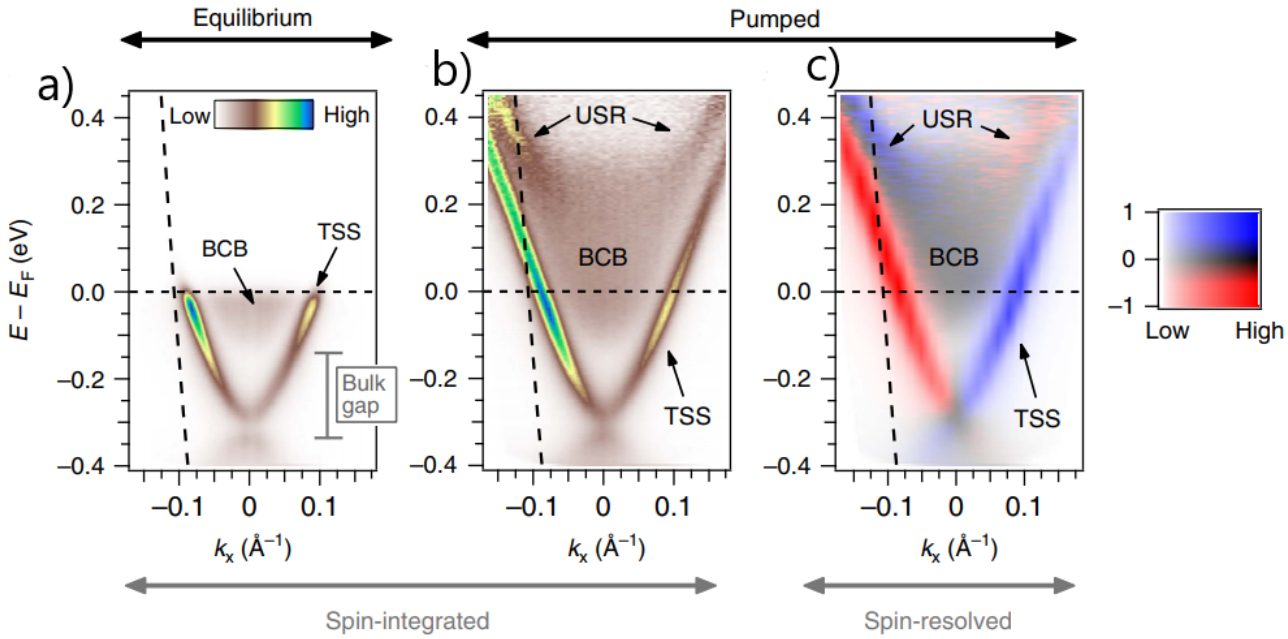

Figure 8: a) Spin-resolved spectra measuring the equilibrium states of Bi_2Se_3 taken along $k_x = 0$ with has no spin resolution. The color bar represents intensity of photo-emission. (b) The same spectrum as in a), but with "pump" which optically excites electrons into previously unoccupied states above the Fermi energy. (c) SR-ARPES spectra of after the optical pumping, the two dimensional colour scheme represents the intensity where bold (faded) corresponds to high (low) intensity and colour corresponding to spin polarization asymmetry measured in the y direction following a cut through the gamma point along $\vec{k}_x$ [19].

With this picture we can imagine probing states with ARPES to construct such a band map throughout the Brillouin zone. Utilizing spin resolution we can gain more information about each band. Specifically we will be able to determine what spin states comprise the bands if there exist such spin polarization. Thus probing energy eigenstates outside of the gamma point one expects to see an asymmetry of spin up and spin down states.

Indeed spin polarization is experimentally observed. Jozwiak *et al.* performed SR-ARPES on Bi_2Se_3 which confirmed a spin polarized band structure of the TSS within the bulk gap. Data can been seen in Figure 8, which confirms the existence of topological surfaces states below E_F with ARPES. This measurement allows one to picture the relatively high density of states of the TSS bands compared to the BCB.

It is often beneficial to use an an optical pump to excite electrons into states above E_F which yields insight into the dispersion of the TSS and their relative intensities, data of such a measurement is pictured in Figure 8. Most importantly spin resolved ARPES was used to detect the spin polarization of each band. As expected from a topological material, the TSS are spin split as indicated by the red-blue colour map.

Another way to visualize c) in Figure 8 is through the intensity vs $\vec{k}_x$ vector as shown in Figure 9. Here the asymmetry in spin intensity (red(blue) triangles indicating spin up(down) in the y basis) is precisely shown as the difference in the two sets of data, which can then be related to the intensity of the dispersion curves in Figure 8. These cuts across the gamma point are also above the Dirac point as pictured in Figure 8 b). If the measurements are carried out while probing at lower energy (below the Dirac point pictured in b)) one would observe spin polarization opposite to that observed above the Dirac point. In other words the positive $\vec{k}_x$ values would be red. As an aside the hexagonal Brillouin zone is pictured indicating a hexagonal Wigner-Seitz cell as expected.

The spin states of various $\vec{k}$ values can be deduced from the spin intensity data along any cut

through the gamma point i.e. if a cut is made in any direction through the gamma point in the x,y plane in any direction oppositely polarized states in the TSS bands are observed. Thus spin locked states can be pictured as states where the spin polarization is orthogonal to the k vector at all points along the Fermi surface. These states are commonly referred to as helical Dirac states.

The utility of SR-ARPES has been demonstrated using a topologically insulating material which can be used to realize new physics in many condensed matter systems. This technique allows researchers to observe the spin helical structure caused by band inversion which splits spin up and spin down states into individual bands.

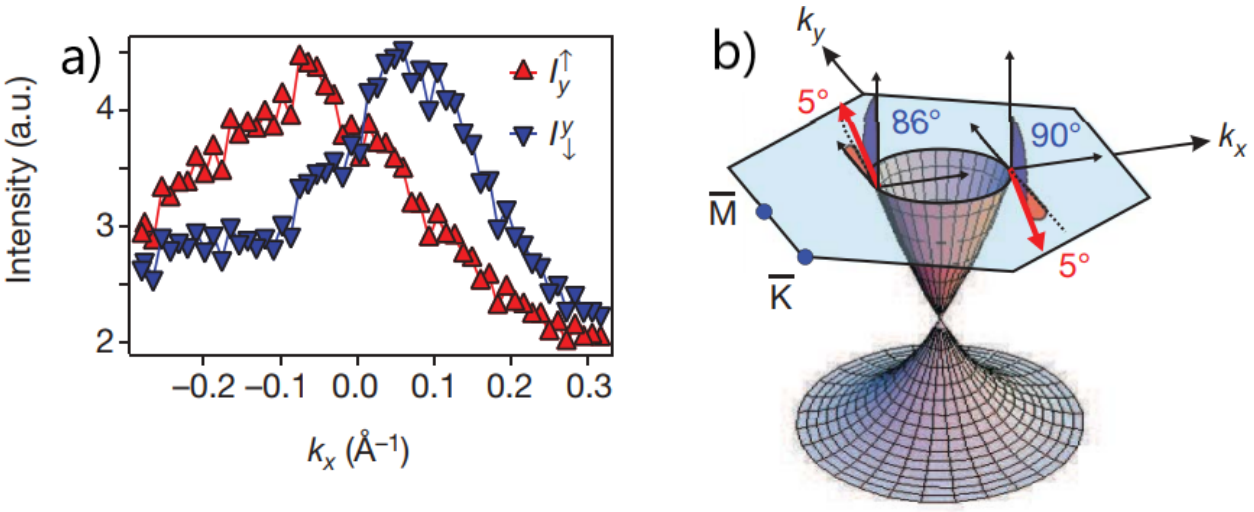

Figure 9: A Spin-resolved spectra measuring the asymmetry in spin polarization along a cut along k_x through the gamma point. Spin polarization is measured in the y direction. The spin dependent states can be deduced from the spin intensity data which demonstrates the spin helical surface states [20].

References

[1] S. Hufner. "Photoelectron Spectroscopy", *Springer Series in Solid State Sciences*, pp 244–284 (1995)

[2] A. Damascelli. "Probing the Electronic Structure of Complex Systems by ARPES", *Physica Scripta*, 61 (2004)

[3] S. Suga, A. Sekiyama. "Photoelectron Spectroscopy", *Springer Berlin Heidelberg*, pp 7–31 (2014)

[4] E. Beaurepaire, H. Bulou, F. Scheurer, J. P. Kappler. "Magnetism: A Synchrotron Radiation Approach", *Springer Berlin Heidelberg*, pp 97–103 (2006)

[5] Settimio Mobilio, Federico Boscherino, Carlo Meneghini. "Synchotron Radiation" *Springer* (2015)

[6] Riccardo Comin, Andrea Damascelli. "ARPES: A Probe of Electronic Correlations" *Springer Berlin Heidelberg* (2015)

[7] K.C. Westfold. "The Polarization of Synchrotron Radiation" *Astrophysical Journal* 130 (1959)

[8] Giuseppe Dattoli *et al.* "Linac-based free electron laser devices: oscillator and single passage operating modes" *Charged Beam Dynamics, Particle Accelerators and Free Electron Lasers, IOP Publishing.* (2017)

[9] Wentao, Zhang. "Photoemission Spectroscopy on High Temperature Superconductor" *Springer* (2013)

[10] J.D. Koralek *et al.* "Experimental setup for low-energy laser-based angle resolved photoemission spectroscopy" *Review of Scientific Instruments, vol. 78* (2007)

[11] Guodong Liu *et al.* "Development of a vacuum ultraviolet laser-based angle-resolved photoemission system with a superhigh energy resolution better than 1meV" *Review of Scientific Instruments, vol 79.* (2008)

[12] M.P. Seah, W.A. Dench. "Quantitative electron spectroscopy of surfaces: A standard data base for electron inelastic mean free paths in solids" *Surface and Interface Analysis* (1979)

[13] X.J. Zhou *et al.* "Space charge effect and mirror charge effect in photoemission spectroscopy" *Journal of Electron Spectroscopy and Related Phenomena* (2005)

[14] R.F. Egerton. "Electron Energy-Loss Spectroscopy in the Electron Microscope" *Springer* (2011)

[15] A de St. Croix. "Xenon Differential Cross-Section: Kinematics" *Carleton University* (2017)

[16] M. Dogun *et al.* "Double Differential Cross-Sections for Electron Impact Ionization of Atoms and Molecules" *Journal of Spectroscopy* ID 192917 (2013)

[17] A. Damascelli, Z. Shen, Z. Hussain. "Angle-resolved photoemission spectroscopy of the cuprate superconductors" (2002) arXiv:cond-mat/0208504

[18] A. Takayami. "High-Resolution Spin-Resolved Photoemission Spectrometer and the Rashba Effect in Bismuth Thin Films" *Springer Theses* (2015)

[19] D. Hsieh et al."Spin-polarized surface resonances accompanying topological surface state formation" *Nature* (2009)

[20] Chris Jozwiak et al. "Spin-polarized surface resonances accompanying topological surface state formation" *Nature Communications* (2016)

Appendix

Momentum Relations

The perpendicular component of momentum can be found by accounting for electron diffraction through the surface barrier. Let θ_i be the angle of the electrons wave-vector $\vec{k}_f$ with respect to the surface normal. The electron will be transmitted through a barrier V_0, which will then decrease the overall perpendicular momentum component $K_\perp$, meaning the conservation of energy in the perpendicular direction gives

$$k_{f,\perp} = \sqrt{\frac{2m(E_k \cos^2(\theta) + V_0)}{\hbar^2}} \tag{8}$$

Fermi's Golden Rule

ARPES experiments rely on the photoelectric effect, so we will consider the effects of incident radiation $\vec{A}(\vec{r}, t)$ on an N-electron system $\Psi_i^{(N)}$, where $\Psi_i^{(N)}$ is an eigenstate of the unperturbed Hamiltonian. Suppose the radiation excites one of the N electrons initially in state $\phi_i(\vec{k}_i)$ to the state $\phi_f(\epsilon_k, \vec{k})$. The cumulative initial and final N-electron states can then be written as $\Psi_i^{(N-1)}\phi_i(\vec{k}_i)$, and $\Psi_f^{(N-1)}\phi_f(\epsilon_k, \vec{k})$, respectively. The transition probability per unit time between these states in the presence of a perturbation $\hat{H}_{int} = \frac{\hbar e}{mc}\vec{A}\cdot\hat{\vec{p}}$ is given by Fermi's Golden Rule as

$$w_{i\to f} \propto |\langle \Psi_f^{(N-1)}\phi_f(E_{kin}, \vec{k})|\, \hat{H}_{int}\, |\Psi_i^{(N-1)}\phi_i(\vec{k}_i)\rangle\,|^2 \delta(E_f - E_i - h\nu) \tag{9}$$

where $h\nu$ is the energy is the incident light [1]. In separating the photoelectrons state from the (N-1)-electron final state, we have used what is referred to as the 'sudden approximation'. This assumes that the photoelectron is immediately decoupled from the remaining (N-1)-electron state $\Psi_f^{(N-1)}$ upon excitation, before relaxation occurs. Further, we will assume $\Psi_f^{(N-1)}$ can be expressed as the sum of all eigenstates of the perturbed Hamiltonian $\Psi_{f,s}^{(N-1)}$ with energy $E_s^{(N-1)}$, i.e., $\Psi_f^{(N-1)} = \Sigma_s c_s \Psi_{f,s}^{(N-1)}$. Assuming a dipole approximation ($\vec{A} \propto e^{ikr}, e^{ikr} \approx 1$), we can re-write Eq. 9 as

$$\begin{aligned} w_{i\to f} &\propto \Sigma_s |\langle \Psi_{f,s}^{(N-1)}|\Psi_i^{(N-1)}\rangle\,|^2 |\langle \phi_f(\epsilon_k, \vec{k})|\,(\vec{\epsilon}\cdot\vec{r})\,|\phi_i(\vec{k}_i)\rangle\,|^2 \delta(E_f - E_i - h\nu) \\ &= \Sigma_s |c_{i,s}|^2 |M_{i,f}|^2 \delta(E_f - E_i - h\nu) \end{aligned}$$

where $\vec{\epsilon}$ is the polarization vector of the incident field, $M_{i,f} = \langle \phi_f(\epsilon_k, \vec{k})|\,(\vec{\epsilon}\cdot\vec{r})\,|\phi_i(\vec{k}_i)\rangle$, and $c_{i,s} = \langle \Psi_{f,s}^{(N-1)}|\Psi_i^{(N-1)}\rangle$. Therefore the total transition rate (often called spectral intensity or photocurrent) $I = \Sigma_{i,f} w_{i\to f}$ can be written as

$$I \propto \Sigma_{i,f,s} |M_{i,f}|^2 |c_{i,s}|^2 \delta(\epsilon_k + E_s^{(N-1)} - E_i^{(N)} - h\nu) \tag{10}$$

Eq. 10 applies to atoms and molecules, but for solids, we define a continuous function $A(\vec{k}, \omega)$, called the spectral function, which accounts for all electron, phonon, and magnon excitations associated with the creation of a hole with wavevector $\vec{k}$. It is convenient to re-write Eq.10 as $I(\vec{k}, \omega) \propto \Sigma_{i,f,s} |M_{i,f}|^2 A(\vec{k}, \omega)$ the physical meaning of $A(\vec{k}, \omega)$ is given by

$$A(\vec{k}, \omega) = -\frac{1}{\pi}\,\mathrm{Im}(G(\vec{k}, \omega)) \tag{11}$$

where ϵ_k^0 be the one-electron energy, and

$$G(\vec{k}, \omega) = \frac{1}{\hbar\omega - \epsilon_k^0 - \Sigma(\vec{k}, \omega)} \tag{12}$$

Accounting for the self-energy, the spectral function becomes

$$A(\vec{k},\omega) = \frac{1}{\pi}\frac{\mathrm{Im}(\Sigma(\vec{k},\omega))}{(\hbar\omega - \epsilon_k^0 - \mathrm{Re}(\Sigma(\vec{k},\omega)))^2 + \mathrm{Im}(\Sigma(\vec{k},\omega))^2}$$

(13)